Materials Research Proceedings 28 (2023) 467-476 https://doi.org/10.21741/9781644902479-51

Yield stress and work hardening behavior of extruded AA6082 profiles under different homogenization and extrusion conditions

WILLIAMS William M.[1,a], SANDNES Lise[1,b], MA Jun[1,c], TRONVOLL Sigmund Arntsønn[1,d] and WELO Torgeir[1,e *]

[1]Norwegian University of Science and Technology (NTNU), Department of Mechanical and Industrial Engineering, Richard Birkelands vei 2B, Trondheim, Norway

[a]william.m.williams@ntnu.no, [b]lise.sandnes@ntnu.no, [c]jun.ma@ntnu.no, [d]sigmund.tronvoll@ntnu.no, [e]torgeir.welo@ntnu.no

Keywords: Aluminum Extrusion, Thermo-Mechanical History, Work Hardening

Abstract. The mechanical properties of extruded AlMgSi alloys are affected by the applied thermo-mechanical parameters employed during the entire production process. In the following, the effect of different extrusion speeds and homogenization conditions paired with either air or water quenching, is examined on four different sets of rectangular hollow AA6082-T4 profiles. These profiles were fabricated and extruded under industrial conditions and selected cross sections of each profile were examined by optical microscopy to determine the microstructure and level of recrystallization. Uniaxial tension testing was used to explore the effect of homogenization conditions and extrusion cooling rate on mechanical properties. Tensile tests showed that the water-quenched extrusions had a higher yield and ultimate strength compared to air-quenched extrusions. Moreover, samples that had a recrystallized microstructure typically showed a larger standard deviation of mechanical properties, which may lead to product quality and consistency issues for metal forming operations. Overall, the present work provides a more in-depth understanding of how the selected thermo-mechanical parameters affect the resulting properties of such profiles. This can further contribute to expanding the potential for effective accommodation of extrusion parameters for zero-defect products.

Introduction

Aluminum alloys, such as the AlMgSi alloys, are commonly used for structural applications in the form of extruded products as they allow for customizing cross sectional geometry with efficient use of material. This allows the profile geometry to be tailored for the specific application area, and the production process tailored to the geometry [1]. The resulting mechanical properties of such aluminum profiles are affected by the entire production process, including the alloy chemical composition and the applied thermo-mechanical history, from casting to final product [2]. As industry pushes towards the goals of reducing climate impact, increasing process adaptability and product customization, deeper understanding of the interactions of different manufacturing process-steps is required to fully utilize the favorable properties of aluminum extrusions.

Stretch bending of aluminum profiles is a commonly used forming method for producing lightweight products [3]. However, a variety of challenges are related to such forming processes particularly for industrial applications; e.g., springback, tool wear, and geometric defects [4]. In order to improve the fabrication process and the prediction of the material response during stretch bending, there is a need for an accurate model of the work hardening behavior. Moreover, an accurate model is critical for predicting geometric recovery such as springback after forming, allowing for adaptive processes which can compensate for this behavior. Recently, Ma et al. [5], have shown that an accurate prediction of the forces during forming is possible provided the material hardening behavior is known. With this information, tool wear can be modeled and maintenance schedules can be developed. Moreover, Ma and Welo [6] have recently used

analytical methods to assess the springback problem for aluminum profiles. In their work, they have shown how springback calculation can become quite complex for complicated bend geometries with variable stress states along the profile length. In their analysis, the stress state is a function of position along a cross section with stress gradients developing through transition zones and becoming stable in a uniform bending zones. When the forming process reaches the point where the entire material cross section is in the plastic state, the stress gradient will decrease as the flow stress curve approaches the saturation stress of the model [6]. Thus, once a specific part geometry is considered and the material hardening behavior is properly modeled, Ma and Welo's method can be applied in combination with finite element methods to predict springback and final part geometry of stretch bended aluminum extrusions.

Using process and property models which can account for the thermo-mechanical history to determine production parameters can allow for optimization of material and energy use by more holistic design methods. Furu et al. [7] propose a modeling framework which connects several independent models of separate process steps together. Thus, optimization of certain AlMgSi alloys, such as AA6082, by simulation is now possible with respect to several key factors such as properties and cost. Accurate prediction of dispersoid development during homogenization is critical to prediction of material structure, properties, and thus responses to later process steps with models by Dons et al. [8] and Dons [9] predicting these material characteristics. For example, the strength of AA6xxx alloys is affected by dispersoid size and density as it can determine the precipitation development during both natural (NA) and artificial aging (AA) as shown by Myhr et al. [10, 11]. This framework can also account for work hardening effects due to dislocation strengthening from pre-strain as shown by Granum et al. [12], and it is possible that this modeling family can be expanded to more accurately predict the hardening behavior of AlMgSi alloys.

However, the deformation experienced during extrusion also lead to further effects on properties. Schikorra et al. [13] divided extruded material into shear intensive zones (SIZs) or a main deformation zone (MDZ), with the higher strain and strain rates of the SIZ leading to higher potential for dynamic recrystallization during extrusion. Per Zhang et al. [14], during dynamic recrystallization grain size is a function of temperature and strain rate, and Schikorra et al. argued that this is a result of a critical strain value being reached, while Van Geertruyden et al. [15] suggests that it is based on deformation energy stored in the material from the extrusion process. Both the previous works are focused on PCG surface layers, but work by Wang et al. [16] shows that internal weld seams behave similarly. Extrusion bridge designs which increased strain also increased recrystallization of an AA6082-type alloy, consistent with the work on PCG surface layers. Similarly, work by Birol [17] shows that by increasing the number density of dispersoids (by increasing Cr and Zr) recrystallization was reduced along weld seams of extruded 6082 tubes.

The effects of homogenization parameters on dispersoid density are not limited to recrystallization, as dispersoid density effects the response of 6xxx series aluminums to aging. Work by Rakhmonov et al. [18] explains how a higher density of smaller dispersoids then resulted in an increase in β'' particles after AA, and thus improved strength. The developed as a result of alloying elements still present in solid solution, rather than in non-strengthening dispersoids. This understanding is in line with the reduction in quench sensitivity with NA found by Strobel et al. [19] in a study focused on high dispersoid density 6xxx series alloy. Alternatively, it was shown by Frodal et al. [20] that lower cooling rate decreases yield strength, due to an increase in the size of precipitate free zones around dispersoids and grain boundaries in multiple T6 aged 6xxx series alloys.

In short, variations in early extrusion production steps, such as homogenization treatment, cooling after extrusion and ageing conditions, may change the material response to downstream processes like subsequent forming operations. This work seeks to provide an example data set for the process modeling community where critical details of the material history and process

parameters are known, the mechanical properties measured, and potential impacts on downstream processes considered. The current work will show how process steps, which change the microstructure of extruded profiles, result in changes to the mechanical behavior of the material. As a result, this work will present data necessary for the process and property modeling community to move forward.

Methods

Homogenization and Extrusion.

Four sets of AA6082.26 profiles were extruded at Benteler Automotive Raufoss AS, employing differing homogenization and extrusion parameters, as listed in Table 1. and shown schematically in Fig. 1. All profiles are extruded from a single log with the composition measured at casting, as listed in Table 2. Sample sets are labeled based on their homogenization parameters and extrusion speed (either S or L) and the quenching fluid after extrusion (either A or W). Billets were homogenized for either 2.25 hours at 530°C (samples S) or for 12 hours at 590°C (samples L) before extrusion. The profiles used for this study are taken from four extrusions, with 2 prior extrusions used to ensure that all equipment was at stable operating temperature and providing stable operation conditions. Prior to extrusion, billets are heated to 470°C and then extruded at either 7 m/min (samples S) or 10 m/min (samples L). After extrusion, either forced air quenching (samples A) was applied over 40 meters after extrusion exit or water spray quenching (samples W) over 10 meters, with all extrusions reaching a temperature near 65°C after these processes. All extrusions had an extrusion ratio of 55, and the profile nominal cross-section dimensions are 60 × 40 mm with a wall thickness of 3 mm. A schematic of the profile cross section is shown in Fig. 2. Note that the extruded profiles under four sets of parameter combinations are labeled individually as SA, LA, SW, and LW.

Table 1. Homogenization and extrusion parameters for materials used for this study, all extrusions are AA6082.26.

Extrusion	1	2	3	4
Homogenization Temp [°C]	530	590	530	590
Homogenization Time [hours]	2.25	12	2.25	12
Extrusion Speed [m/min]	7	10	7	10
Quenching Fluid	Air	Air	Water	Water
Sample Label	SA	LA	SW	LW

Table 2. Composition of AA6082.26 extrusions used for this study.

Al	B	Ni	Cr	Cu	Fe	Si	Mg	Mn	Ti	V	Zn	Zr
97.5	0.004	0.002	0.145	0.0025	0.151	0.921	0.628	0.5155	0.0215	0.0145	0.0435	0.001

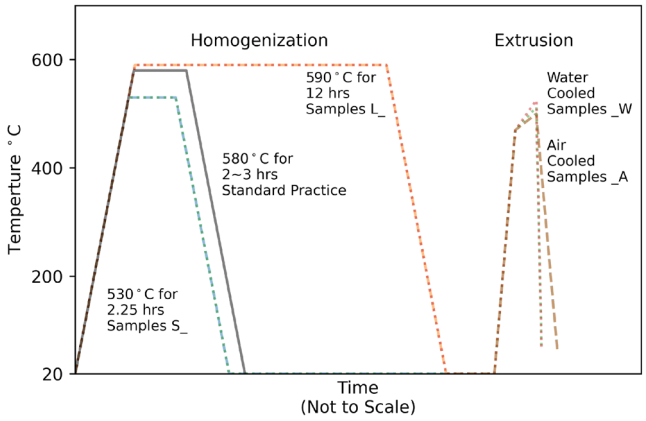

Fig. 1. Schematic of homogenization and extrusion temperatures over time with specific parameters varied for this study shown (dashed lines, also given in Table 1), in comparison to industry standard process parameters [21] shown with the solid line.

Microscopy.

Optical microscopy (OM) was done to characterize the level of recrystallization. OM imaging was done on corner sections of the extrusion cross section, with the extrusion direction normal to the image plane using a Zeiss Axio Vert Inverted Light Microscope with a 5x lens. Fig. 2 shows the image plane position and orientation with respect to the extrusion direction. OM surfaces were polished to 1 µm and anodized at room temperature in Baker's reagent (10 ml HBF_4 (48%) + 400 ml distilled water) for 90 seconds before imaging. OM images have a resolution of 0.685 µm/px, with image stitching used to show the full cross sections.

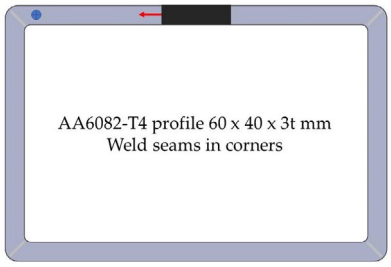

(a) Hollow Rectangular Profile Cross Section

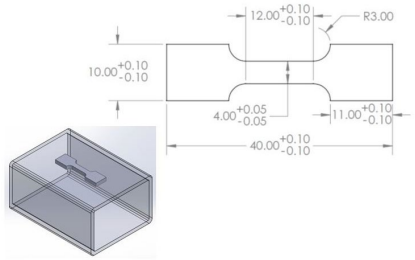

(b) Mechanical Test Sample Dimensions and Position

Fig. 2. Cross section of rectangular hollow extrusions (a) and location of samples within cross section with dimensions of uniaxial tension samples (b). The blue arrow in (a) indicates the surface normal of the OM images of extrusion cross sections.

Tensile Tests.

Subsize tensile test samples were machined from the profiles with a so-called dogbone geometry, having a nominal cross-section of 3 x 4 mm and a gauge length of 12 mm. The position of the samples with respect to profile geometry is according to the schematic shown in Fig. 2. In order to determine possible variation, 3 samples along the same flange of a profile were used for testing. Uniaxial tension tests of the samples were done with an initial nominal strain rate of 0.001 1/s using an Instron ElectroPuls E10000 servo-electric load frame. Digital image correlation (DIC) [22] *in-situ* measurement of material deformation was used with Correlated Solutions VIC-Snap 8 and VIC-2D 7 software. Strain measurement was done using virtual extensometers within the

DIC data set. The engineering strain is used for determining uniform elongation, ultimate tensile strength (UTS), and an offset strength (OFS) at 0.002. This offset is chosen for ease of comparison to the Voce initial stress value explained below. The true plastic strain is calculated, with the elastic strain component removed using a Young's modulus of 70 GPa [23]. As AA6082 shows soft knee yielding and determining individual moduli per sample is highly sensitive to experimental setup and selection of data points, the single reference value was used for all samples. A Voce-type hardening model (Eq. 1) is then fit to the material behavior up to 20% plastic strains, ϵ^p, as given by:

$$\sigma_{True} = K + Q * \left(1 - e^{(-b\epsilon^p)}\right) \quad (1)$$

where σ_{True} is true flow stress, K is the initial stress value, Q is the saturation stress value, and b is the hardening exponent.

The plastic anisotropy ratio, r, is calculated at ϵ^p = 5% in the loading direction and is thus r_0, not to be confused with normal and planer anisotropies $\underline{R}$ and ΔR respectively. The calculation uses the nearest measured longitudinal plastic strain to ϵ^p = 5% and the corresponding measured lateral plastic strain. From these measured strains, the thickness plastic strain is calculated assuming incompressibility. 5% plastic strain was chosen as a representative point considering the range of plastic strains experienced during stretch bending [24].

Results

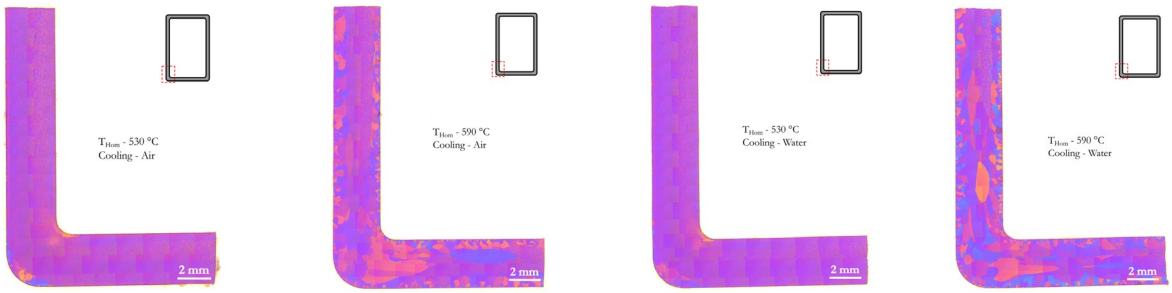

(a) Extrusion SA (b) Extrusion LA (c) Extrusion SW (d) Extrusion LW

Fig. 3. Optical microscopy imaging of the cross sections of AA6082.26 with variable extrusion histories as given in Table 1. Extrusion direction is out of the image plane.

Microstructure.

OM images of the cross sections are presented in Fig. 3, and show a fibrous grain structure is present in some part of all extrusions, with a peripheral coarse grain (PCG) layer in both the LA and LW extrusions. There is PCG growth in the corners of SA and SW, though it does not extend through the profile thickness along the weld seams. Note that the depths of the PCG layer for the LA extrusion are not symmetric on the inner and outer surfaces of the profile. The level of recrystallization in the LW cross section resulted in a thicker PCG layer in comparison to the LA extrusion. The difference in the recrystallization behavior between the T_{Hom}=530°C (S) and T_{Hom}=590°C (L) extrusion pairs is consistent with expectations based on dispersoid density after their respective homogenization parameters. Differences in recrystallization between extrusion pairs based on cooling method are still noticeable in Fig. 3, though less significant. As stated above, a fibrous-grained core is still present in both LA and LW samples. For the LA and LW cross sections, there is also recrystallization of the core within the profile corner with a PCG layer consisting of grains that are smaller than the recrystallized core. So, a PCG layer covers both the interior and exterior surfaces of the L extrusion profiles over 2 "core" areas with a fibrous core in the central areas of the webs and flanges and a recrystallized core in the corners.

Materials Research Proceedings 28 (2023) 467-476 https://doi.org/10.21741/9781644902479-51

Mechanical Properties.

The experimental flow stresses (σ_{True} vs plastic true strain ϵ^p) sorted by extrusion are shown in Fig. 4 with the curves ending at UTS. As expected and shown in Fig. 4, the material response varied based on both homogenization and cooling parameters. Water quenched extrusions; i.e., those with a higher cooling rate, showed a higher initial flow stress as reflected in both the stress-strain, $\sigma_{True} - \epsilon^p$, curves of Fig. 4 and the Voce initial strength K shown in Fig. 5 (d). The average OFS of the water-quenched extrusions (162.2 MPa and 152.1 MPa, for extrusions SW and LW respectively), as shown in Fig. 6 (a), is higher than the air-quenched extrusions (137.7 MPa and 139.3 MPa for extrusions SA and LA respectively). This difference is not dramatic, but with a variance ratio (between group variance/within group variance) of 17.34 it is greater than the difference between samples from the same extrusion. UTS showed a more significant difference between the water-quenched samples (258.6 MPa and 248.5 MPa for extrusions SW and LW respectively) and air-quenched samples (221.2 MPa and 232.8 MPa for extrusions SA and LA respectively), as shown in Fig. 6 (a). The UTS variance ratio is 46.14, which reflects a stronger relationship between an extrusion's thermo-mechanical history and UTS compared to OFS. This trend is also reflected in the saturation stress Q of the Voce model, shown in Fig. 5 (b).

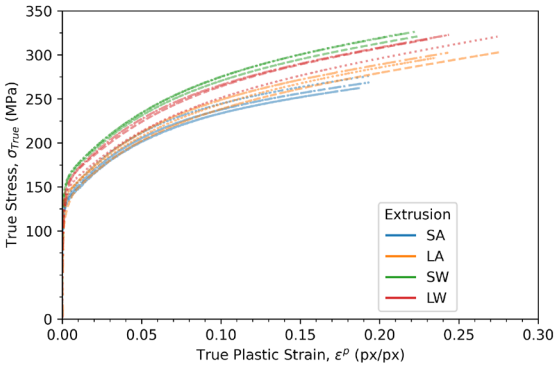

*Fig. SEQ Figure * ARABIC 4. Experimental true stress vs plastic true strain of AA6082.26 with varied thermo-mechanical histories as explained and labelled in Table 1.*

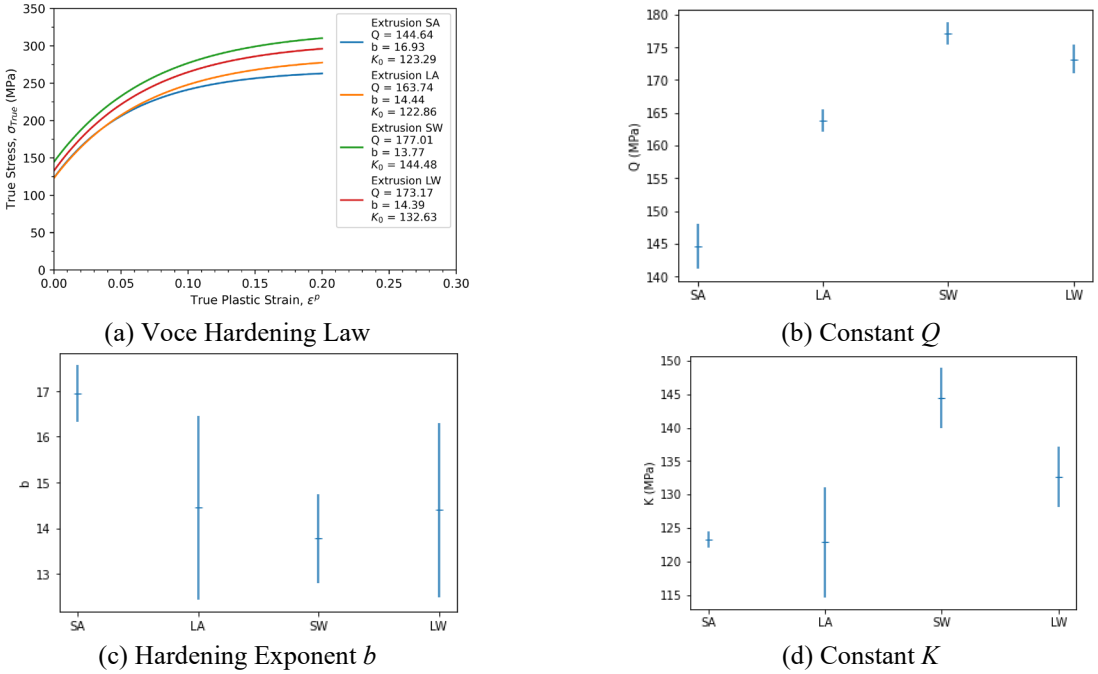

(a) Voce Hardening Law (b) Constant Q

(c) Hardening Exponent b (d) Constant K

Fig. 5. Fit of a Voce like hardening law to experimental true stress vs plastic true strain data of AA6082.26 with varied thermo-mechanical histories as given in Table 1. The Voce like hardening law is plotted for each extrusion in (a) using the constant Q (b), hardening exponent b (c), and constant K (d).

In contrast to strength, the ductility of the samples is better sorted by homogenization parameters than by cooling rate. The uniform elongation, as shown in Fig. 6 (b), is higher for both L sample sets, but the standard deviation (SD) is larger. In contrast, the level of consistency in both UTS and flow stress curves shown in Fig. 4 for both S extrusions is notable. It is important to observe that this trend is however not reflected in the strain to failure, in comparison to uniform elongation. The SW extrusion had similar failure strains as that of the L samples, implying significant elongation after UTS.

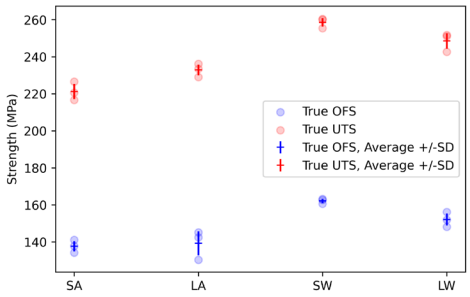

(a) Ultimate Strength (UTS) and 0.002 Offset Strength (OFS)

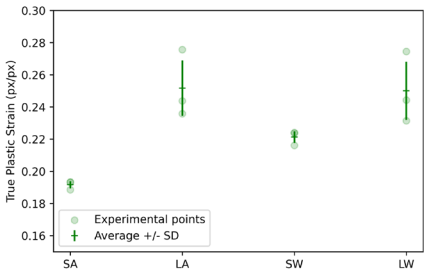

(b) Uniform Elongation

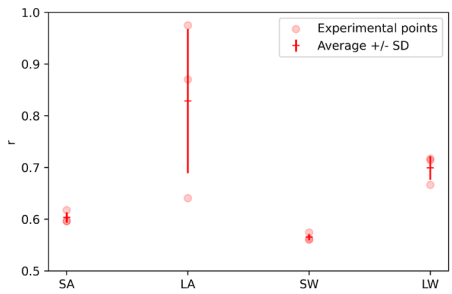

(c) Plastic Ratio *r*

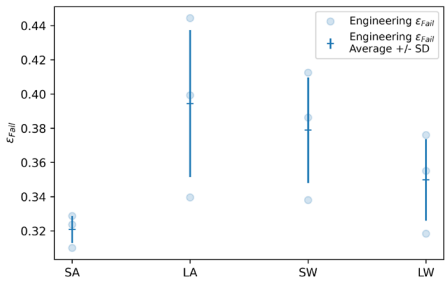

(d) Engineering Strain at Failure

Fig. 6. Mechanical properties of AA6082.26 T4 with variable extrusion histories as given in Table 1. Ultimate Tensile strength (UTS) and 0.002 offset strength (OFS) are shown in (a), uniform elongation in (b), plastic ratio r at 5% plastic strain in (c), and engineering failure strain in (d).

Discussion

As shown in the results section higher extrusion speeds in combination with homogenization parameters, and thus a lower number density of dispersoids, increases the recrystallization in AA6082 extrusions. On thin wall profiles, such as hollow rectangular extrusions, this can result in a significant portion of the cross section being PCG or recrystallized. This difference in material microstructure changes mechanical behavior, especially initial yielding, plastic deformation, and work hardening, due to the influence of grain size and texture on these properties.

Considering the recrystallization of the L extrusions, primarily within the different portions of a cross section, recall the work of Schikorra *et al*. [13]. Their framework is helpful to understand the differences between the PCG around the surface of the L cross sections, the fibrous core, and the coarser recrystallized grains in the corners as shown in Fig. 3. The higher recrystallization in combination with the higher extrusion speeds of the L samples is consistent with understandings presented above in [14], [15]. However, these results suggest that the material making up the corners does not fit cleanly within either SIZ or MDZ categories. Also, material which is within the same category of SIZ on the internal and external surfaces are not similar thicknesses, which is consistent with the different deformation histories of each. Thus, further work is needed to investigate the material flow path within this particular toolset to clarify the link between

deformation history and recrystallization. Based on Wang et al. [16], it is reasonable that the higher strain experienced by the material from the MDZ in the corners is resulting in the coarser grain growth. It also explains why there is also recrystallization in the S cross section corners, while the majority of the cross section retains a fibrous microstructure. In short, the PCG layer recrystallization is driven by strain history as part of the SIZ of the extruded material which is consistent around all surfaces. In the corners, a recrystallized core from the MDZ develops as a result of a longer flow path than the fibrous core. Thus it is also possible that the material making up the corners does not fit within either SIZ or MDZ categories.

As stated in the results section above, the mechanical characteristics of the profiles have a stronger relationship to the extrusion cooling rate than the homogenization parameters. However, it is clear from both the literature and differences between the SW and LW extrusions that the homogenization parameters have an effect. This work examines NA AA6082, and as such β' particles develop at nucleation points (which are often dispersoids [19]). Alloying elements which would have developed into β'' particles during AA remain in solid solution, strengthening the material. While Frodal et al. [20] was of AA rather than NA 6xxx series, it is consistent with this understanding of the results. The SW samples had higher UTS and OFS than LW samples, as well as higher average Voce constants Q and K as shown in Fig. 6 (a), Fig. 5 (b) and (d) respectively.

It is also interesting to note from these figures that both recrystallized extrusions LA and LW had higher uniform elongations and r at 5% ϵ^p, likely due to the recrystallized grain structure within these extrusions. Both characteristics suggest the LA and LW extrusions would have better formability, as r approaching 1 implies more isotropy and higher uniform elongations imply a larger allowable strain range for forming before localization. However, for both of these characteristics, the SD of the tested samples are larger than for the S samples (and in the case of r for LA, larger than the LW samples) which suggests possible production consistency issues. While these characteristics might imply better forming performance, recrystallized profiles tend to have an "orange peel" like surface texture which may cause issues for parts and profiles that must meet surface quality requirements for either paint or appearance for surfaces visible to the end user. It is also important to note that while the mechanical properties of initial flow stress and UTS of the LW samples were higher than both SA and LA samples, the SW extrusions are the best performing for applications where maximum mechanical strength is needed based on the extrusions tested.

Summary

Four sets of AA6082.26 rectangular hollow profiles are produced using industrial equipment and methods, using differing homogenization and extrusion parameters. Both microstructural characteristics and mechanical properties of the extruded profiles were examined. The influences of thermo-mechanical history on the property of extruded profiles were discussed. The main conclusions are summarized as follows:

- Extrusions with longer time and higher temperature homogenization resulted in higher levels of uniform elongation and more isotropic plastic deformation regardless of extrusion cooling rate.
- Higher extrusion cooling rates led to higher strengths overall (both ultimate and offset strengths), with this effect being larger in extrusions with shorter homogenization time.
- The hardening behavior of the material up to 20% plastic strain can be represented regardless of homogenization or extrusion parameters using a Voce like hardening law for the flow stress behavior.
- Extrusions with longer time and higher temperature homogenization showed higher standard deviations across a number of mechanical parameters, including hardening exponent b, plastic ratio r, and uniform elongation.

Based on these results, the extrusion cooling rate is more critical to control than recrystallization with respect to mechanical characteristics. For process modeling, homogenization effects on

ductility due to microstructural composition and the effect of extrusion cooling rate on strength are the primary effects of each process which then interact to result in the hardening behavior. Further work can proceed along two lines, either via investigation of the material or investigation of the subsequent forming process. Investigation of the material would involve TEM imaging and measurement of dispersoid size and density, as well as β' precipitate development during natural aging. Work proceeding along the forming process would show the impact of these property variations on dimensional accuracy of formed parts.

Acknowledgments
This work was funded by the Research Council of Norway project AdaptAl - Adaptive Control of Aluminum Manufacturing (project number: 314054), and supported by the NTNU Aluminum Product Innovation Center (NAPIC).

References
[1] D.H. Ko, B.H. Kang, D.C. Ko, B.M. Kim, Improvement of mechanical properties of Al6061 extrudate by die cooling with N2 gas during hot extrusion, J. Mech. Sci. Technol. 27 (2013) 153-161. https://doi.org/10.1007/s12206-012-1213-x
[2] S.K. Fjeldbo, Y. Li, K. Marthinsen, T. Furu, Through-process sensitivity analysis on the effect of process variables on strength in extruded Al-Mg-Si alloys, J. Mater. Process. Technol. 212 (2012) 171-180. https://doi.org/10.1016/j.jmatprotec.2011.08.020
[3] J. Cao, M. Banu, Opportunities and challenges in metal forming for lightweighting: Review and future work, J. Manuf. Sci. Eng. Trans. ASME 142 (2020) 1-24. https://doi.org/10.1115/1.4047732
[4] A.E. Tekkaya, P.O. Bouchard, S. Bruschi, C.C. Tasan, Damage in metal forming, CIRP Ann. 69 (2020) 600-623. https://doi.org/10.1016/j.cirp.2020.05.005
[5] J. Ma, T. Welo, G. Ringen, Efficient Prediction of Real-Time Forming Forces in Flexible Stretch Bending, Esaform 2021, no. April, 2021. https://doi.org/10.25518/esaform21.4040
[6] J. Ma, T. Welo, Analytical springback assessment in flexible stretch bending of complex shapes, Int. J. Mach. Tools Manuf. 160 (2021). https://doi.org/10.1016/j.ijmachtools.2020.103653
[7] T. Furu, R. Østhus, J. Søreide, O.R. Myhr, A Novel Methodology for Optimization of Properties, Costs and Sustainability of Aluminium Extrusions, Mater. Sci. Forum 877 (2016) 625-632. https://doi.org/10.4028/www.scientific.net/MSF.877.625
[8] A.L. Dons, E.K. Jensen, Y. Langsrud, E. Trømborg, S. Brusethaug, The alstruc microstructure solidification model for industrial aluminum alloys, Metall. Mater. Trans. A Phys. Metall. Mater. Sci. 30 (1999) 2135-2146. https://doi.org/10.1007/s11661-999-0025-9
[9] A.L. Dons, The Alstruc homogenization model for industrial aluminum alloys, J. Light Met. 1 (2001) 133-149. https://doi.org/10.1016/S1471-5317(01)00007-4
[10] O.R. Myhr, Ø. Grong, K.O. Pedersen, A combined precipitation, yield strength, and work hardening model for Al-Mg-Si alloys, Metall. Mater. Trans. A Phys. Metall. Mater. Sci. 41 (2010) 2276-2289. https://doi.org/10.1007/s11661-010-0258-7
[11] O.R. Myhr, Ø. Grong, C. Schäfer, An Extended Age-Hardening Model for Al-Mg-Si Alloys Incorporating the Room-Temperature Storage and Cold Deformation Process Stages, Metall. Mater. Trans. A Phys. Metall. Mater. Sci. 46 (2015) 6018-6039. https://doi.org/10.1007/s11661-015-3175-y
[12] H. Granum, O.R. Myhr, T. Børvik, O.S. Hopperstad, Effect of pre-stretching on the mechanical behaviour of three artificially aged 6xxx series aluminium alloys, Mater. Today Commun. 27 (2021). https://doi.org/10.1016/j.mtcomm.2021.102408
[13] M. Schikorra, L. Donati, L. Tomesani, A.E. Tekkaya, Microstructure analysis of aluminum extrusion: Grain size distribution in AA6060, AA6082 and AA7075 alloys, J. Mech. Sci. Technol. 21 (2007) 1445-1451. https://doi.org/10.1007/BF03177357

[14] C. Zhang, C. Wang, R. Guo, G. Zhao, L. Chen, W. Sun, X. Wang, Investigation of dynamic recrystallization and modeling of microstructure evolution of an Al-Mg-Si aluminum alloy during high-temperature deformation, J. Alloys Compd. 773 (2019) 59-70. https://doi.org/10.1016/j.jallcom.2018.09.263
[15] W.H. Van Geertruyden, H.M. Browne, W.Z. Misiolek, P.T. Wang, Evolution of surface recrystallization during indirect extrusion of 6xxx aluminum alloys, Metall. Mater. Trans. A Phys. Metall. Mater. Sci. 36 (2005) 1049-1056. https://doi.org/10.1007/s11661-005-0298-6
[16] Y. Wang, A. Zang, Y. Mahmoodkhani, M. Wells, W. Poole, N. Parson, The Effect of Bridge Geometry on Microstructure and Texture Evolution During Porthole Die Extrusion of an Al–Mg–Si–Mn–Cr Alloy, Metall. Mater. Trans. A Phys. Metall. Mater. Sci. 52 (2021) 3503-3516. https://doi.org/10.1007/s11661-021-06322-5
[17] Y. Birol, Effect of Cr and Zr on the grain structure of extruded en AW 6082 alloy, Met. Mater. Int. 20 (2014) 727-732. https://doi.org/10.1007/s12540-014-4018-x
[18] J. Rakhmonov, K. Liu, P. Rometsch, N. Parson, X.G. Chen, Effects of Al(MnFe)Si dispersoids with different sizes and number densities on microstructure and ambient/elevated-temperature mechanical properties of extruded Al–Mg–Si AA6082 alloys with varying Mn content, J. Alloys Compd. 861 (2021) 157937. https://doi.org/10.1016/j.jallcom.2020.157937
[19] K. Strobel, M.A. Easton, M.D.H. Lay, P.A. Rometsch, S. Zhu, L. Sweet, N.C. Parson, A.J. Hill, Quench Sensitivity in a Dispersoid-Containing Al-Mg-Si Alloy, Metall. Mater. Trans. A Phys. Metall. Mater. Sci. 50 (2019) 1957–1969. https://doi.org/10.1007/s11661-019-05130-2
[20] B.H. Frodal, E. Christiansen, O.R. Myhr, O.S. Hopperstad, The role of quench rate on the plastic flow and fracture of three aluminium alloys with different grain structure and texture, Int. J. Eng. Sci. 150 (2020) 7491. https://doi.org/10.1016/j.ijengsci.2020.103257
[21] O. Reiso, Extrusion of AlMgSi alloys, Mater. Forum 28 (2004) 32-46.
[22] H. Schreier, J.-J. Orteu, M.A. Sutton, Image Correlation for Shape, Motion and Deformation Measurements, Boston, MA: Springer US, 2009.
[23] HYDRO, Technical datasheet - Extruded products Alloy EN AW - 6082 [AlSi1MgMn], Hydro, 2019, 3-5.
[24] T. Welo, J. Ma, J. Blindheim, T. Ha, G. Ringen, Flexible 3D stretch bending of aluminium alloy profiles: An experimental and numerical study, Procedia Manuf. 50 (2020) 37-44. https://doi.org/10.1016/j.promfg.2020.08.008